Plant Physiology Preview. Published on September 12, 2017, as DOI:10.1104/pp.17.00971

Short title: Lack of *At*tDT has little effect on stomata

***Corresponding author:**

Wagner L. Araújo

Departamento de Biologia Vegetal,

Universidade Federal de Viçosa,

36570-900 Viçosa, Minas Gerais, Brazil

E-mail: wlaraujo@ufv.br

Tel: +55 31 3899.2169; Fax**:** +55 31 3899.2580

Research Area: Biochemistry and Metabolism

Article type: Research article

Title: Impaired malate and fumarate accumulation due to the mutation of the tonoplast dicarboxylate transporter has little effects on stomatal behaviour

Authors: David B. Medeiros[1,2,3], Kallyne A. Barros[1,2], Jessica Aline S. Barros[1,2], Rebeca P. Omena-Garcia[1,2], Stéphanie Arrivault[3], Lílian M.V.P. Sanglard[2], Kelly C. Detmann[2], Willian Batista Silva[1,2], Danilo M. Daloso[3§], Fábio M. DaMatta[2], Adriano Nunes-Nesi[1,2], Alisdair R. Fernie[3], Wagner L. Araújo[1,2]*

[1]*Max-Planck Partner Group at the Departamento de Biologia Vegetal, Universidade Federal de Viçosa, 36570-900, Viçosa, Minas Gerais, Brazil*

[2]*Departamento de Biologia Vegetal, Universidade Federal de Viçosa, 36570-900, Viçosa, Minas Gerais, Brazil*

[3]*Max Planck Institute of Molecular Plant Physiology, 14476 Potsdam-Golm, Germany*

One-sentence summary: Manipulation of tonoplastic organic acid transport by inhibition of the tDT impacts mitochondrion metabolism, whilst the overall stomatal and photosynthetic performance is not affected.

Key words: organic acids; growth; primary metabolism; respiration, stomata

Footnotes:

[§]Present address: *Departamento de Bioquímica e Biologia Molecular, Universidade Federal do Ceará, Fortaleza, Ceará, Brasil.*

Author contributions:

DBM, ARF, and WLA designed the research; DBM performed most of the research with the support of KAB, JASB, RPOG, SA, LMVPS, and KCD; WBS, DMD, ANN, and FMD contributed new reagents/analytic tools; ANN, FMD, and SA analysed the data, discussed the results and complemented the writing; DBM, ARF, and WLA analysed the data and wrote the article which was later approved by all the others.

Funding information

This work was supported by funding from the Max Planck Society, the CNPq (National Council for Scientific and Technological Development, Brazil, Grant 402511/2016-6),

and the FAPEMIG (Foundation for Research Assistance of the Minas Gerais State, Brazil, Grant APQ- 01078-15 and APQ-01357-14) to WLA. Scholarship granted by FAPEMIG to DBM (BDS-00020-16), CNPq to KAB and JASB, as well as research fellowships granted by CNPq-Brazil to ANN and WLA are also gratefully acknowledged.

Abstract

Malate is a central metabolite involved in a multiplicity of plant metabolic pathways, being associated with mitochondrial metabolism and playing significant roles in stomatal movements. Vacuolar malate transport has been characterized at the molecular level and is performed by at least one carrier protein and two channels in Arabidopsis vacuoles. The absence of the *Arabidopsis thaliana* tonoplast Dicarboxylate Transporter (tDT) in *tdt* knockout mutant was previously associated with an impaired accumulation of malate and fumarate in leaves. Here, we investigated the consequences of this lower accumulation on stomatal behaviour and photosynthetic capacity as well as its putative metabolic impacts. Neither the stomatal conductance (g_s) nor the kinetic responses to dark, light or high CO_2 were highly affected in *tdt* plants. In addition, we did not observe any impact on stomatal aperture following incubation with either abscisic acid (ABA), malate or citrate. Further, an effect on photosynthetic capacity was not observed in the mutant lines. However, leaf mitochondrial metabolism was affected in the *tdt* plants. Levels of the intermediates of the tricarboxylic acid cycle were altered and increases in both light and dark respiration were observed. We conclude that manipulation of the tonoplastic organic acid transporter impacted mitochondrial metabolism, while the overall stomatal and photosynthetic capacity were unaffected.

Introduction

Malate is a central metabolite in all plant species fulfilling a multiplicity of functions as both an intermediate of the tricarboxylic acid (TCA) cycle (Fernie et al., 2004) and carbon skeletons exported from the mitochondrion supporting amino acid biosynthesis (Tronconi et al., 2008). Malate is also involved in several processes including cellular pH regulation (Hurth et al., 2005), partial control over nutrient uptake (Weisskopf et al., 2006), aluminium tolerance (Delhaize et al., 2007), pathogen response (Bolwell et al., 2002), and stomatal movements (Hedrich et al., 1994). Moreover, it has been demonstrated to be a transcriptional regulator in metabolite signalling (Finkemeier et al., 2013), an important carbon storage molecule in C3 plants (Zell et al., 2010), and a key component of photosynthesis in C4 and CAM plants (Maier et al., 2011).

The vacuolar malate transport, which has been characterized at the molecular level, is thought to be essential to maintain normal cellular function (Emmerlich et al., 2003). First, the gene encoding the vacuolar malate transporter, a plant homolog to the human sodium ion/dicarboxylate cotransporter, the tDT (tonoplast Dicarboxylate Transporter), was identified in *Arabidopsis*. The *tDT* knockout mutants are deficient in vacuolar malate transport activity, exhibited substantially reduced levels of malate and fumarate in the leaves and isolated vacuoles from these mutants were highly impaired in the import of [^{14}C]-malate yet respired exogenously applied [^{14}C]-malate faster than WT plants (Emmerlich et al., 2003). However, in contrast to its homolog in animal cells, the plant protein resides at the tonoplast and transport of malate by the tDT is not sodium-dependent (Emmerlich et al., 2003). In addition, Hurth et al. (2005) demonstrated that tDT is critical for the regulation of pH homeostasis under altered pH conditions. These authors further suggested that Arabidopsis vacuoles contain at least two types of carrier proteins and a channel for transport of dicarboxylates and citrate, thus providing the metabolic flexibility needed by plants to respond to different environmental circumstances. A member of the Aluminium-malate transporter family (ALMT), the ALMT9, was the first channel characterized to mediate malate and fumarate currents directed into the vacuole of mesophyll cells in Arabidopsis (Kovermann et al., 2007). However, it was later demonstrated to mediate malate-induced chloride currents that are also important for stomatal opening (De Angeli et al., 2013). A second member of the ALMT family, ALMT6, mediates Ca^{2+}- and pH-dependent malate currents into guard cell vacuoles (Meyer et al., 2011). Despite *ALMT6*

112 expression is much higher in guard cells than in the mesophyll suggesting an important
113 role of this channel in stomatal movements, no obvious stomatal or growth phenotype
114 was observed under optimal growth conditions (Meyer et al., 2011).

115 Accumulation of malate either in guard cell cytosol and vacuoles or in the
116 apoplastic space can impact stomatal movements and also regulate the activity of anion
117 channels at guard cell plasma or vacuolar membrane (Hedrich and Marten, 1993;
118 Hedrich et al., 1994; Raschke, 2003; Lee et al., 2008; Negi et al., 2008; Kim et al.,
119 2010; De Angeli et al., 2013). Indeed, the role of organic acids (e.g. malate and
120 fumarate) in the regulation of guard cell movements occurs not only by providing the
121 osmotic control but also by playing a critical role in meeting the energetic demand of
122 the guard cells (Santelia and Lawson, 2016). This fact apart, our knowledge about the
123 metabolic hierarchy regulating guard cells movements in response to changes in organic
124 acids remains fragmentary. Interestingly, further evidence supporting the involvement
125 of organic acid metabolism in leaves by linking mitochondrial metabolism and stomatal
126 function have been demonstrated (Nunes-Nesi et al., 2007; Araújo et al., 2011). Tomato
127 (*Solanum lycopersicum* L.) plants with constitutively reduced expression of *SlSDH2-2*
128 which encodes the iron-sulphur subunit of succinate dehydrogenase presented increased
129 stomatal conductance and photosynthesis mediated by organic acids effects on the
130 stomata (Araújo et al., 2011). Importantly, no effects were observed when the antisense
131 construction for *SISDH2-2* was expressed under the control of the guard cell specific
132 *MYB60* promoter (Araújo et al., 2011). By contrast, the constitutive inhibition of the
133 mitochondrial fumarase in tomato plants decreased photosynthesis as a result of
134 impaired stomatal function (Nunes-Nesi et al., 2007).

135 In an attempt to investigate whether the lower levels of malate and fumarate
136 observed in the *tdt* knockout plants has a greater impact on stomatal movement or
137 mitochondrial metabolism in Arabidopsis, we here combined a range of physiological
138 and biochemical approaches. Our results provide evidence that manipulation of organic
139 acid tonoplastic transport by suppressing tDT greatly impact mitochondrial metabolism,
140 but has only minor effects on stomatal and photosynthetic capacity. When considered in
141 the context of current knowledge concerning the compartmentation of these metabolites
142 (Gerhardt et al., 1987; Winter et al., 1993; Hedrich et al., 1994; Martinoia and Rentsch,
143 1994; Winter et al., 1994; Lohaus et al., 2001), this observation suggests that following
144 the mobilisation of the vacuolar malate pool to the cytosol it is preferentially exported
145 to the apoplast and used to support mitochondrial respiration.

146

147

Results

attdt plants exhibit a small reduction in vegetative growth under short-day conditions

Plants lacking a functional tDT display lower levels of malate and fumarate in leaves and isolated vacuoles (Emmerlich et al., 2003; Hurth et al., 2005). Given that these organic acids serve as important carbon storage molecules also in Arabidopsis plants (Zell et al., 2010), we investigated whether loss-of-function of *tDT* affects growth in two independent *tdt* T-DNA insertion lines (*tdt*-1 and *tdt*-2). We initially confirmed the absence of *tDT* transcripts in leaves of the mutants by reverse transcription PCR (Supplemental Fig. S1). Interestingly, no changes in growth were observed under neutral day conditions (12h/12h), with no differences in the rosette fresh weight between WT and *tdt* mutant plants (Supplemental Fig. S2A). However, under short-day conditions (8h/16h) the mutant lines displayed a slightly reduction in their growth being characterized by lower rosette fresh weight (Supplemental Fig. S2B). To investigate further this apparent growth phenotype we evaluated in detail the growth pattern and the metabolism of the genotypes only under short-day conditions. We observed that *tdt* plants presented reductions in the rosette and leaf dry mass (RDM and LDM), total leaf area (LA), rosette area (RA), but no significant differences in specific leaf area (SLA; Table I). We additionally evaluated the stomatal density and stomatal index with both being unaltered in the mutant lines under short-day conditions (Table I).

Lack of tDT has little effect on stomatal response to different stimuli

Altered organic acid accumulation impacts stomatal behaviour coupling mesophyll mitochondrial activity to stomata and, subsequently, to plant growth (Nunes-Nesi et al., 2007; Araújo et al., 2011; Medeiros et al., 2016). To further assess the impact caused by an altered accumulation of malate and fumarate due to the lack of a functional tDT on stomatal conductance (g_s) in Arabidopsis, we adopted the following complementary approaches. First, we evaluated the stomatal kinetics during dark-to-light and light-to-dark transitions as well as following changes from normal-to-high and high-to-normal CO_2 concentrations. Secondly, we evaluated the response of intact leaves following incubation with ABA, malate, fumarate, and citrate individually by isolating epidermal fragments and analysing stomatal aperture. Surprisingly, the impaired accumulation of malate and fumarate in *tdt* leaves did not compromise the stomatal response to dark, light or high CO_2 levels (Fig. 1A-C). Although no statistical

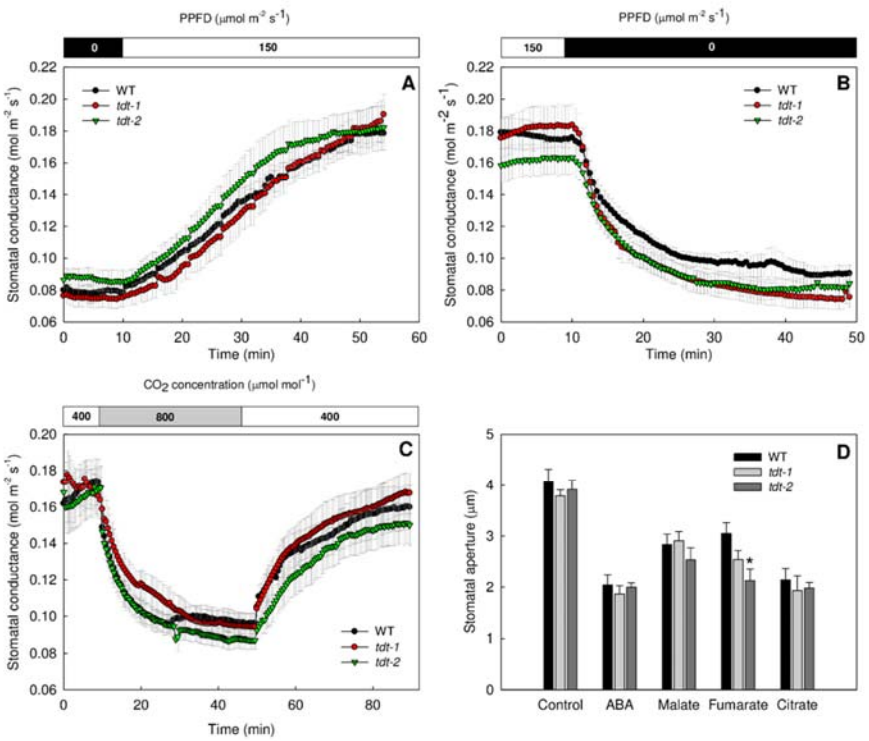

Figure 1. Stomatal responses of *tdt* plant following different stimuli. Stomatal opening and closing kinetics in response to light and CO_2 concentrations. Stomatal conductance (g_s) was evaluated in *tdt-1* and *tdt-2* and WT in response to light **(A)**, dark **(B)** and CO_2 levels **(C)**. Data presented are mean ± SE (n = 10). **D**, Stomatal aperture after incubation with abscisic acid (ABA), malate, fumarate, and citrate. The 5th leaf totally expanded of 4-week-old plants were floated on stomatal opening buffer containing 10 mM KCl, 50 µM $CaCl_2$ and 5 mM MES-Tris (pH 6.15) for 2 h in the light (150 µmol m^{-2} s^{-1}) to pre-open stomata. After, ABA, malate, fumarate, and citrate or ethanol (solvent control) were added to the opening buffer. After more 2 h of incubation the stomatal aperture was then examined in the isolated epidermal fragments. Six leaves from different plants were evaluated and the apertures of at least 20 stomata per leaf were measured totalizing at least 120 stomata per genotype. Data are mean ± SE (n = 6) obtained in two independent experiments with comparable results. Asterisk indicates values that were determined by the Student's t test to be significantly different ($P < 0.05$) from WT.

differences were observed (P<0.05) in response to light, dark, and CO_2 concentration, we estimated the half-times of the stomatal kinetic curves by fitting the time-course of g_s to an exponential model (Martins et al., 2016). Accordingly, the half-times (expressed in min ± SE) for stomatal kinetics curves were also not significantly altered. However, it is noteworthy that the half-time for light-induced stomatal opening in *tdt-2* plants was

lower (8.5 ± 0.7), whereas the values for WT and *tdt-1* plants were 13.2 ± 2.3 and 12.5 ± 1.5, respectively. For dark-induced stomatal closure, the half-times were only slightly reduced in *tdt-1* (4.5 ± 0.6) and *tdt-2* (4.5 ± 0.5) when compared to WT (5.2 ± 1.0). The half-times following high CO_2-induced stomatal closure were also only slightly changed in *tdt-1* (5.0 ± 0.9) and *tdt-2* (4.2 ± 0.5) lines compared to WT plants (3.2 ± 0.5). During the recovery, back to ambient CO_2 concentration (C_a) of 400 μmol mol^{-1}, while *tdt-1* plants appeared to be slightly faster in stomatal opening (8.5 ± 1.6), *tdt-2* and WT presented half-times values of 12.8 ± 2.3 and 13.6 ± 3.9, respectively. Additionally, no effect on the stomatal aperture following the incubation with ABA, malate or citrate was observed (Fig. 1D).

Given that malate can affect *tDT* transcript accumulation (Emmerlich et al., 2003), first, we decided to evaluate whether *tDT* is expressed in guard cells by comparing its expression level in both guard cell-enriched epidermal fragments and isolated mesophyll cell protoplast; second, we measured the transcript levels of currently known genes related to organic and inorganic ion transport as well as genes involved in guard cell movements. For this purpose, we investigated by quantitative real-time PCR (qRT-PCR) the transcript levels of ion channels and transporters in guard cells-enriched epidermal fragments including *ALMT6*, *ALMT9*, *QUAC1*, *ABCB14*, *SLAC1*, *AHA1*, *AHA2*, *AHA5*, *KAT1*, *KAT2*, *AKT1*, *TPC1*, and *GORK* (for a complete description see Materials and Methods and Supplemental Table S1). Regarding the *tDT* expression pattern, our results confirmed previous transcriptome data (Bates et al., 2012), which showed higher expression levels in mesophyll cells than in guard cells (Supplemental Fig. S3 and Supplemental Fig. S4A). Furthermore, the transcript levels of the vast majority of the evaluated genes were only marginally altered in *tdt* plants (Supplemental Fig.S5).

To provide further information that could explain the lack of stomatal phenotype in *tdt* plants, we next quantified the content of organic acids in the apoplastic fluid. To this end, we collected the apoplastic fluid at the middle of the light period from completely water infiltrated leaves by centrifugation and quantified the absolute levels of fumarate, malate, and citrate in the apoplastic fraction by gas-chromatography coupled to mass-spectrometry technique (GC-MS). The unchanged fumarate, malate, and citrate levels in the apoplastic fluid (Fig. 2), probably best explains the lack of effect on stomatal function, since the apoplastic solute concentration is of pivotal significance in driving stomatal movements.

Figure 2.

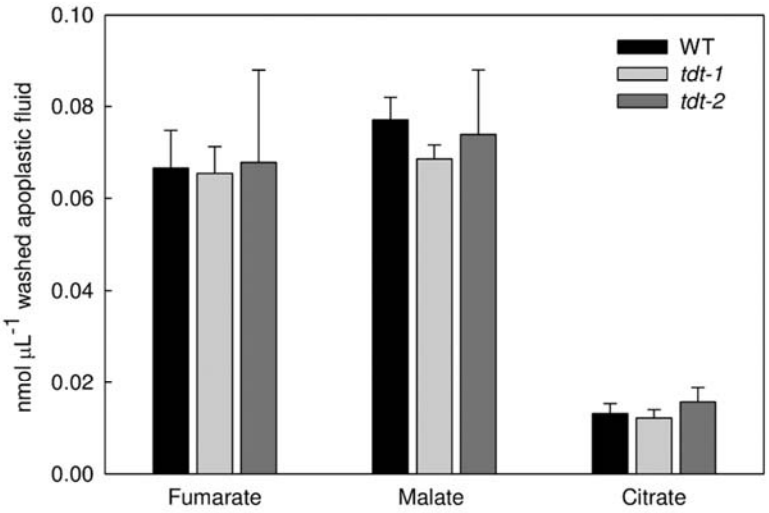

Figure 2. Apoplastic concentrations of organic acids in *tdt* plants. The apoplastic concentrations of fumarate, malate, and malate were determined as described in Material and Methods section. Values are presented as means ± SE of six individual determinations per genotype. All measurements were performed in 5-week-old plants.

221

222 **Photosynthetic capacity is not altered in *tdt* mutant plants**

223 We decided to perform a full characterization of the photosynthetic capacity of
224 *tdt* plants. In close agreement with the stomatal kinetics, no differences were observed
225 in instantaneous gas exchange parameters under either growth irradiance (Table II) or

saturation irradiance (Supplemental Table S2). By further analysing A_N under photosynthetically active photon flux density (PPFD) that ranged from 0 to 1200 µmol m^{-2} s^{-1}, we observed that mutant plants exhibited unaltered A_N irrespective of the irradiance (Supplemental Table S3). The light-saturated A_N (A_{PPFD}), light saturation (I_s) and compensation (I_c) points, and light use efficiency remained similar among the genotypes (Supplemental Table S3). Additionally, the response of A_N to the internal CO_2 concentration (A_N/C_i curves; Supplemental Fig. S6A) was obtained and then were further converted into responses of A_N to chloroplastidic CO_2 concentration (A_N/C_c curves; Supplemental Fig. S6B). Under ambient CO_2 concentration (400 µmol mol^{-1}), C_i and C_c estimations in *tdt* lines were similar to those of the WT (Supplemental Table S4). g_m, estimated by a combination of gas exchange and chlorophyll *a* fluorescence parameters using two independent methods, remained unaltered in *tdt* plants (Supplemental Table S4). Accordingly, the maximum carboxylation velocity (V_{cmax}) and maximum capacity for electron transport rate (J_{max}) was also similar between WT and mutant lines both as a function of C_i and C_c (Supplemental Table S4).

Mutations in *tDT* affect starch, organic acid, and amino acids profiles in both leaves and guard cells

Given that tDT was previously shown to be important for the maintenance of cellular homeostasis, specifically under situations of altered cellular pH (Hurth et al., 2005), we decided to explore the metabolic changes in *tdt* plants by conducting a detailed metabolic analysis in leaves and in enriched-guard cell epidermal fragments of the mutants and WT plants. There were no significant changes in the levels of chlorophylls (Supplemental Fig. S7). Similarly, during the light/dark cycle changes were not observed in the leaf levels of glucose, fructose, and sucrose between mutant and WT plants (Supplemental Fig. S8). However, starch metabolism in the leaves was strongly affected in *tdt* plants during the diurnal cycle (Fig. 3A). Notably, the average starch synthesis and degradation rates were estimated as the difference between starch at the end of the day and the end of the night, divided by the length of the light period or the night, respectively. Starch synthesis rate were 53% (1.43 µmol glc g^{-1} FW h^{-1}) and 46% (1.64 µmol glc g^{-1} FW h^{-1}) lower in *tdt-1* and *tdt-2* plants, by comparison to the WT (3.04 µmol glc g^{-1} FW h^{-1}), respectively. For starch degradation rates the values were on average 59% (0.64 µmol glc g^{-1} FW h^{-1}) and 48% (0.82 µmol glc g^{-1} FW h^{-1})

Figure 3

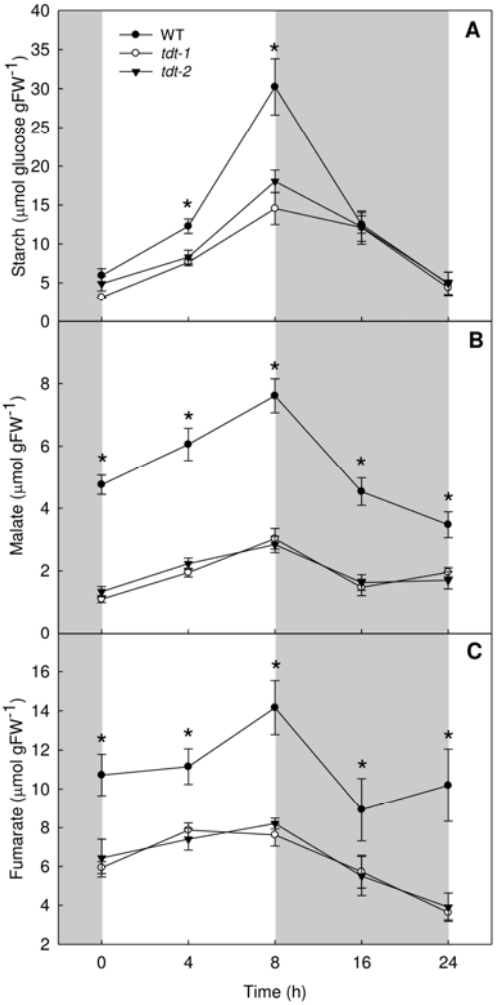

Figure 3. Starch and organic acid content in WT and *tdt* plants. **A** starch; **B** malate; and **C** fumarate content in whole rosettes harvested in different time points along of the light/dark cycle. Values are presented as mean ± SE (n = 6) and asterisk indicates the time where the values from mutant lines were determined by the Student's t test to be significantly different ($P < 0.05$) from WT.

lower in *tdt-1* and *tdt-2* plants than in WT ones (1.58 µmol glc g^{-1} FW h^{-1}), respectively. It should be remembered that lower levels of starch observed in *tdt* plants were not accompanied by any change A_N.

Impaired accumulation of malate and fumarate was previously observed in *tdt* mutants leaves (Emmerlich et al., 2003; Hurth et al., 2005). We additionally evaluated

the malate and fumarate accumulation/usage pattern (Fig. 3). Further, by combining non-aqueous fractionation (NAF) and quantification by enzymatic assays and GC-MS we were able to estimate their subcellular distribution as well as of other organic acids (Supplemental Table S6). Regarding the malate and fumarate accumulation during the diurnal cycle it showed a very similar pattern to that observed for starch, with values observed in *tdt* plants being consistently lower than in WT during the entire diurnal cycle. Remarkably, *tdt* plants showed decreases in both malate (Fig. 3B) and fumarate (Fig. 3C) on average of 62% and 44% at the end of the light period. Interestingly, malate was the only organic acid showing differences in its subcellular distribution. Whereas citrate, isocitrate, and fumarate were predominantly found in the vacuoles, malate was significantly reduced in the vacuoles, however increases in malate were observed in the cytosol of the mutant lines (Supplemental Table S6).

We next decided to perform a detailed analysis of the primary metabolism in leaves and in enriched-guard cells epidermal fragments by using the established GC-MS approach (Lisec et al., 2006). This analysis revealed that, among the 48 successfully annotated compounds, considerable changes in amino acids, and in both TCA cycle and photorespiratory intermediaries were observed (Fig. 4; Supplemental Table S5). By analysing individual amino acids, we observed significant increases in leaves for both lines in asparagine (Asn), aspartate (Asp), and lysine (Lys) levels as well as the branched chain amino acids (BCAAs) leucine (Leu), isoleucine (Ile), and the aromatic amino acid tyrosine (Tyr) was also increased in the *attdt* plants. Notably, glycolate and glycine (Gly), intermediates of the photorespiratory pathway, were significantly decreased in leaves, whereas glutamine (Gln) levels increased in mutant plants in both leaves and guard cells. The levels of some organic acids found in the first half of the TCA cycle citrate (only in leaves) and isocitrate (in both leaves and guard cells) were strongly increased while succinate, fumarate, and malate were reduced in mutant lines only in leaves. Other changes of note observed in the metabolite profile were the significant increases in *myo*-inositol and reduction in maltose levels in leaves in both lines. Intriguingly, significant increases were observed in the levels of glucose, fructose, and trehalose in guard cells.

We next evaluated whether the metabolic perturbations observed were accompanied by changes in the activity of important enzymes in leaves, which are associated with glycolysis and carbohydrate metabolism (Table III). Interestingly, the maximum activity of phosphoglycerate kinase (PGK), pyruvate kinase (PK), and

Figure 4.

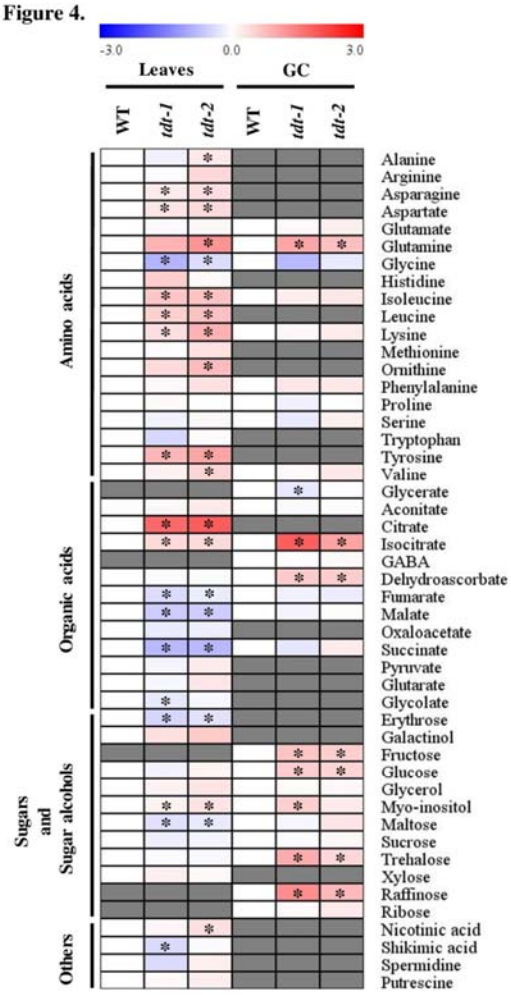

Figure 4. Heat map representing the changes in relative metabolite content in leaves and guard cell-enriched epidermal fragments from WT and *tdt* plants. The full data sets from these metabolic profiling studies are additionally available in Supplemental Table S5. The colour code of the heat map is given at the log(2) following the scale above the diagram. Data are normalized with respect to the mean response calculated for WT (to allow statistical assessment, individual plants from this set were normalized in the same way). Values are presented as means ± SE (n = 5). Asterisks indicate that the values from mutant lines were determined by Student's t test to be significantly different ($P < 0.05$) from WT. In grey, the metabolites which were not detected or could not be annotated.

1

298 aldolase (significantly only for *tdt-2*) were higher in *tdt* than in WT plants. There were
299 no changes in the activity of hexokinase (HK), phosphofructokinase (PFK), enolase or
300 triose phosphate isomerase (TPI). Similarly, transaldolase and glucose-6-phosphate
301 dehydrogenase (G6PDH), both related to the pentose phosphate pathway, and sucrose

synthase were unaltered in *tdt* plants. However, the activity of acid invertase was decreased in the mutant lines.

tdt knockout plants present altered flux through the TCA cycle

We decided to directly assess the respiration rate by performing two complementary approaches. First, we directly evaluated the rate of light respiration in the mutant lines by measuring the $^{14}CO_2$ evolution following incubation of leaf discs with positional-labeled ^{14}C-glucose (^{14}C-Glc) molecules to assess the relative rate of flux through the TCA cycle. For this, we incubated leaf discs under light supplied with either [1-^{14}C]-Glc or [3,4-^{14}C]-Glc over a period of 6 h. During that period, we collected the $^{14}CO_2$ evolved at hourly intervals. CO_2 can be released from the C1 position by the action of enzymes that are not associated with mitochondrial respiration, but CO_2 released from the C3,4 positions of glucose cannot (Nunes-Nesi et al., 2007). Therefore, the ratio of CO_2 evolution from C3,4 to C1 positions provides a reliable indication of the relative rate of the TCA cycle versus other carbohydrate oxidation processes. By comparing the $^{14}CO_2$ release from mutant lines to WT plants we observed that significant increases occurred only for *tdt-2* line after 5 h of incubation following incubation with [1-^{14}C]-Glc (Fig. 5A), whereas when supplied with [3,4-^{14}C]-Glc the $^{14}CO_2$ release was significantly increased in both mutant lines from 4 h onwards (Fig. 5B). In addition, the C3,4/C1 ratio was higher in mutant lines than in WT plants after 6 h incubation (Fig. 5C), revealing that a higher proportion of carbohydrate oxidation was performed by the TCA cycle in illuminated leaves. Furthermore, the higher dark respiration (R_d), measured by using an infra-red gas analyser system, revealed higher rates of CO_2 evolution in the leaves of *tdt* plants than in the WT (Fig. 5D).

Figure 5.

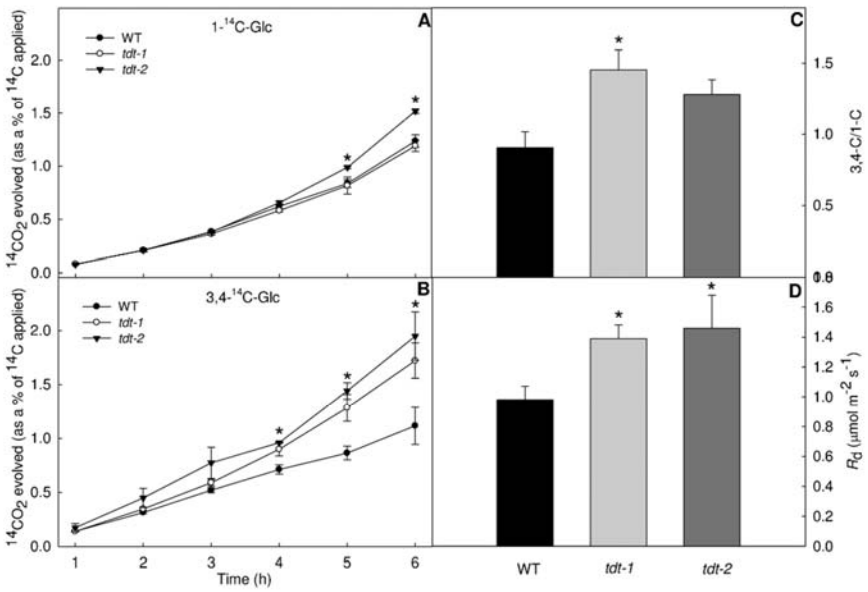

Figure 5. Respiration parameters in leaf disks from WT and *tdt* plants. $^{14}CO_2$ evolution from isolated leaf discs was determined under light conditions. The leaf discs were taken from 5-week-old plants and incubated in 10 mm MES–KOH solution, pH 6.5, 0.3 mM Glucose (Glc), 0.1 mM $CaSO_4$ supplemented with 0.62 kBq mL^{-1} of **(A)** [1-^{14}C]-Glc; or **(B)** [3,4-^{14}C]-Glc at an irradiance of 100 µmol m^{-2} s^{-1}. The $^{14}CO_2$ released was captured (at hourly intervals) in a KOH trap and the amount of radiolabel released was subsequently quantified by liquid scintillation counting. **C**, Ratio of carbon dioxide evolution from C3,4 to C1 positions of Glc in leaves of *tdt* plants. Values are presented as means ± SE (n = 3) **D**, Dark respiration measurements performed on 5-week-old plants. Values presented are mean ± SE (n = 10) obtained in two independent assays (five plants in each assay). An asterisk indicates values that were determined by the Student's t test to be significantly different ($P < 0.05$) from the WT plants.

Discussion

Functional absence of tDT does not alter stomatal movements and photosynthetic capacity

To evaluate the reasons underlying the growth impairment observed in *tdt* plants under short-day conditions (Supplemental Fig. S1 and Table I), we decided to

investigate whether the impaired organic acid accumulation affected stomatal function and thereby photosynthetic capacity in these plants. We were somewhat surprised to find that the growth phenotype was independent of changes in stomatal density, stomatal index, and photosynthetic capacity (Table I; Table II; Supplemental Fig. S6; Supplemental Table S2; S3; S4). Collectively, these results indicate that guard cell function is not highly affected in *tdt* plants (Fig. 1), and the stomata were most likely able to reprogram their metabolism to overcome the impaired vacuolar malate storage observed previously (Emmerlich et al., 2003) and confirmed here during the entire diurnal cycle and in the non-aqueous fractionation experiments (Fig. 3 and Supplemental Table S6). Notably, although tDT is essential for mediating correct compartmentation of the dicarboxylates, *tdt* plants still exhibit residual malate importing activity (Emmerlich et al., 2003; Hurth et al., 2005). It has been suggested that tDT is the major transporter responsible for malate and fumarate through the tonoplast in mesophyll cells (Hurth et al., 2005); however, members of the ALMT family are also implicated in this function as malate channels in plants. For instance, ALMT6 which is more expressed in guard cells than in the mesophyll ones (Supplemental Fig. S3) was shown to mediate Ca^{2+}- and pH-dependent malate currents into guard cell vacuoles, suggesting that it could be the main vacuolar transport system for organic acids in guard cells (Meyer et al., 2011). Because this channel does not exhibit sufficient activity to accumulate dicarboxylates at concentrations required for normal metabolic functioning it may not be able to fully compensate the absence of tDT in mesophyll cells (Hurth et al., 2005). Furthermore, ALMT9 was first observed to mediate malate and fumarate currents directed into the vacuole, it was later shown to mediate malate-induced chloride current, which is also important for stomatal opening (Kovermann et al., 2007; De Angeli et al., 2013). Notably, our gene expression analyses did not reveal any significant difference at the mRNA levels of ALMT6 and ALMT9 between WT and *tdt* plants (Supplemental Fig. S5).

We previously demonstrated that there is a negative correlation between the apoplastic levels of malate and fumarate and both stomatal aperture and gas exchange in tomato antisense lines for genes encoding fumarase and succinate dehydrogenase enzymes (Araújo et al., 2011). Consistent with the lack of change in stomatal function, in the current study we did not observe any change in apoplastic levels of fumarate, malate, and citrate (Fig. 2). In keeping with this, it is highly tempting to suggest that although malate and fumarate cannot be properly accumulated in the vacuoles due the

lack of a functional tDT transporter, the majority of these compounds produced need to be further redistributed within the cell. This would support the proper stomatal function by the maintenance of apoplastic concentrations of organic acids even with decreased total amounts in the leaves (Fig. 3). Moreover, it also indicates that these compounds are highly metabolized by the TCA cycle (Fig. 5), as previously suggested (Emmerlich et al., 2003). Thus, it seems that mitochondrial metabolism, especially of those pathways associated with malate, has great potential to improve photosynthesis, and growth ultimately, most likely through a better control of stomatal movements (Nunes-Nesi et al., 2011). That said it remains to be elucidated whether the functional redundancy in the vacuolar organic acid transport in guard cells is responsible for lack of stomatal phenotype in *tdt* plants.

Lower growth in *tdt* plants was not related to impairments in the photosynthetic capacity

A detailed photosynthetic characterization revealed that the lower vegetative growth in *tdt* plants was not due to an impaired photosynthetic capacity. This analysis was necessary despite the lack of change in stomatal behaviour since the rate of CO_2 diffusion through the stomata is not the only constraint to the photosynthetic performance in plants and the pathway to CO_2 diffusion from stomata to the Rubisco carboxylation sites in the chloroplasts can become an important limiting factor to the photosynthetic process as well as the Rubisco carboxylic capacity (Gerhardt et al., 1987; Martins et al., 2013). Our results demonstrated an invariable instantaneous net CO_2 assimilation in *tdt* plants both under growth irradiance and light saturation (Table II and Supplemental Table S2). This was also observed when we estimated the photosynthetic capacity from response curves of A_N to C_i or C_c as well as to PPFD (Supplemental Fig. S6 and Supplemental Table S3 and S4). Arabidopsis plants with highly reduced levels of malate and fumarate due to the overexpression of a maize (*Zea mays*) plastidic NADP-malic enzyme (MEm) exhibited smaller rosettes with decreased biomass accumulation and thinner leaves when compared to WT plants. This was almost certainly the consequence of a reduced photosynthetic performance under short-day conditions in these plants (Zell et al., 2010), suggesting that the long dark period and extremely low levels of malate and fumarate are not sufficient to support the sugar depletion after the usage of carbohydrate stored during the night. Interestingly, these findings were not observed when these plants were grown under long-day conditions

(Fahnenstich et al., 2007). Indeed, the rates of starch and organic acid usage during the night correlate with one another and with the relative growth rate, indicating that although these two carbon sources are independently regulated their utilization is highly coordinated (Fahnenstich et al., 2007; Gibon et al., 2009; Zell et al., 2010; Sulpice et al., 2014; Figueroa et al., 2016; Lauxmann et al., 2016). Although many of the molecular details concerning the connection between starch and organic acid metabolism in governing plant growth are being revealed (Figueroa et al., 2016), deeper elucidation of how plants and in particular crop species adjust their metabolism to support growth will be important and strategic research avenues to be pursued in the near future.

We showed here that *tdt* plants were impaired in their growth under short-day conditions, which can be explained, at least partially, by the reduced malate and fumarate content in the leaves of these plants across the entire diurnal cycle (Fig. 3B and Fig. 3C). Moreover, starch accumulation in *tdt* mutant lines in our growth conditions was negatively affected, with reduced values at the end of the light period (Fig. 3A). It is, therefore, reasonable to assume that *tdt* plants display a carbon-starvation phenotype when grown under SD conditions, given that no visible growth phenotype was observed when we grew these mutant plants under 12h/12h light/dark photoperiod (Supplemental Fig. S2).

Respiratory metabolism is changed as consequence of the *tDT* repression

The impaired malate exchange observed in *tdt* plants has been previously proposed to be able to provoke unknown regulatory reactions at the expense of cytosolic energy equivalents (Emmerlich et al., 2003; Hurth et al., 2005). This assumption was further reinforced by the demonstration that radiolabelled malate fed into mutant leaf discs entered the TCA cycle much faster than in WT tissues (Emmerlich et al., 2003). Furthermore, the observation that *tdt* leaf discs exhibited both an increased respiratory activity and increased respiratory quotient (Hurth et al., 2005) demonstrated the accelerated usage of cytosolic carboxylic acids as an energy source in plants lacking a functional tDT transporter. Here, we provide compelling evidence that the absence of tDT strongly affects the mitochondrial metabolism in vivo. By using complementary approaches, we further confirmed that the slower growth in *tdt* plants was accompanied by enhanced dark and light respiration (Fig. 5), providing more evidence for the connection between the TCA cycle functioning and growth (Nunes-Nesi et al., 2007; Araújo et al., 2011). Tomato plants exhibiting either an antisense inhibition of fumarase

(Nunes-Nesi et al., 2007) or the iron-sulfur subunit of succinate dehydrogenase (Araújo et al., 2011) displayed an impaired mitochondrial metabolism. In these transgenic plants, the flux through the TCA cycle was clearly reduced; however, whereas deficiency in fumarase led to lower CO_2 assimilation and reduction in growth (Nunes-Nesi et al., 2007), the succinate dehydrogenase antisense lines showed higher transpiration and g_s, followed by elevated CO_2 assimilation and growth (Araújo et al., 2011). These differences were both ascribed to the apoplastic levels of malate and fumarate as mentioned above, which were elevated in the fumarase antisense lines and reduced in the succinate dehydrogenase antisense lines (Araújo et al., 2011). That respiratory metabolism was affected in these lines is by no means surprising given that they are directly effected in the TCA cycle. That the *tdt* lines are also affected is highly interesting since it suggests that the TCA cycle is, to a considerable extent, fuelled directly by malate supply, which is accumulated in the cytosol in these plants (Supplemental Table S6). Moreover, it is in keeping with previous suggestions of a non-cyclic flux mode of the TCA cycle in leaves under light conditions (Sweetlove et al., 2010; António et al., 2016). This scenario is further supported by the steady-state levels of the intermediates of the TCA cycle in leaves observed here (Fig. 4 and Supplemental Table S5) and are in good agreement with the high dependence on the metabolic and physiological cell demands associated with organic acid metabolism (Sweetlove et al., 2010).

It is important to highlight that the levels of succinate, fumarate, and malate were decreased in leaves, but not in guard cells of mutant lines (Fig. 4). This observation suggests a different functional importance of the tDT transporter in mesophyll and guard cells, which is in agreement with the differential expression pattern of *tDT*, being more expressed in mesophyll cells than in guard cells (Bates et al. (2012) and Supplemental Fig. S4). Moreover, the high expression of the ALMT6 at the guard cell tonoplast seems to compensate the lack of tDT, at least regarding the proper storage of malate and fumarate in those cells (Fig. 4). Curiously, since we observed a strong accumulation of citrate in leaves and isocitrate in both leaves and guard cells and this accumulation is addressed occurring within the vacuole (Supplemental Table S6), it is tempting to speculate that tDT might also be somehow involved with the compartmentalization of these organic acids. Although we were not able to ascertain in the current study which organic acids are effectively transported by the tDT it will be

interesting to further investigate whether the mitochondrial metabolism in guard cell is also affected when tDT is repressed in future studies.

Collectively, our results suggest that impaired accumulation of malate and fumarate as a consequence of non-functional tDT affects the cellular homeostasis in mesophyll cells by changing mitochondrial metabolism, without negative impacts to the stomatal and photosynthetic behaviours. When the relative concentrations of the apoplastic and subcellular malate pools are considered (Gerhardt et al., 1987; Winter et al., 1993; Hedrich et al., 1994; Martinoia and Rentsch, 1994; Winter et al., 1994; Lohaus et al., 2001), it is tempting to speculate that the impact on mitochondrial metabolism is most likely due to increased consumption of carboxylates within the cell, since it cannot be properly stored into the vacuole. Additionally, transporting the increased cytosolic malate pools for the maintenance of apoplastic levels could be a mechanism by which *tdt* plants maintain the stomatal function. This observation is thus consistent with our previous studies both suggesting that apoplastic malate levels play a crucial role in stomatal function.

Material and methods

Plant material and growth conditions

All *Arabidopsis thaliana* plants used here were of the Wassilewskija ecotype (Ws) background. WT and *tdt* plants were grown in a growth chamber under short-day (8 h/16 h of light/dark) or neutral-day (12 h/12 h of light/dark), irradiance of 150 µmol m^2 s^{-1}, 22ºC/20ºC during the light/dark cycle, and 60% relative humidity. The T-DNA mutant lines *tdt-1* and *tdt-2* were identified by screening a library of T-DNA lines from Arabidopsis Knockout Facility, University of Wisconsin Biotechnology Center (Emmerlich et al., 2003). The abundance of transcripts was confirmed by semi-quantitative PCR, using specific primers pair for *tDT* gene - At5g47560: forward 5′-ACACTACAACATCCATCGCC-3′ and reverse 5′-ATGCATCCACATGCTTACGT-3′. *GLYCERALDEHYDE-3-PHOSPHATE-DEHYDROGENASE* (*GAPDH*) – At1g16300 expression was also evaluated as a control using the following primers pair: forward 5′-TGGTTGATCTCGTTGTGCAGGTCTC-3′ and reverse 5′-GTCAGCCAAGTCAACAACTCTCTG-3′.

Growth analysis

501 Whole rosettes from 5-week-old plants were harvested and the rosette fresh and
502 dry weight (RDW), total leaf area (LA), specific leaf area (SLA) were measured. LA
503 was measured by digital image method using a scanner (Hewlett Packard Scanjet
504 G2410, Palo Alto, CA, USA) and the images were processed using the ImageJ software
505 (Schindelin et al., 2015). SLA were calculated as described in Hunt et al. (2002).
506
507 **Stomatal analysis**
508 After 2 h of illumination in the light/dark cycle, leaf impressions were taken
509 from the abaxial surface of the 5th leaf totally expanded with dental resin imprints
510 (Berger and Altmann, 2000). Nail polish copies were made using a colorless glaze (Von
511 Groll et al., 2002) and the images were taken with a digital camera (Axiocam MRc)
512 attached to a microscope (Zeiss, model AX10, Jena, Germany). The measurements were
513 performed on the images using the AxionVision software (Carls Zeiss, Germany).
514 Stomatal density and stomatal index (the ratio of stomata to stomata plus other
515 epidermal cells) were determined in at least 10 fields of 0.09 mm^2 per leaf from eight
516 different plants. For stomatal aperture assay the 5th leaf totally expanded of 5-week-old
517 plants were floated on stomatal opening buffer containing 10 mM KCl, 50 μM $CaCl_2$
518 and 5 mM MES-Tris (pH 6.15) for 2 h under light (150 μmol m^{-2} s^{-1}) to pre-open
519 stomata. After, ABA, malate, fumarate, and citrate or ethanol (solvent control) were
520 added to the opening buffer to final concentration of 10 μM, 10 mM, 10 mM, 10 mM or
521 0.1 % (v/v), respectively. After 2 h of incubation the stomatal aperture was evaluated.
522 The leaves were gently dried and the adaxial epidermis was carefully fixed to an
523 autoclave tape. The abaxial surface of the leaves were then peeled off by fixing an
524 adhesive film (tesafilm® crystal clear, Tesa, Hamburg, Germany) and the images were
525 immediately taken (Azoulay-Shemer et al., 2015). Six leaves from different plants were
526 evaluated and the aperture of at least 20 stomata per leaf was measured giving a total of
527 at least 120 stomata per genotype.
528
529 **Stomatal opening and closing kinetics measurements**
530 The g_s values were recorded at intervals of 1 min using an open-flow infrared gas
531 exchange analyser system (LI-6400XT; LI-COR Inc., Lincoln, NE) equipped with
532 an integrated fluorescence chamber (LI-6400-40; LI-COR Inc.). The g_s responses to
533 dark/light and light/dark transitions were measured in plants acclimated to dark or light,
534 for at least 2 h. The light in the chamber was kept turned off, and then turned on for

10/40 min and turned on/turned off 10/40 min. The CO_2 concentration in the chamber was kept at 400 µmol mol^{-1} air. For responses to CO_2 concentration transitions leaves were exposed to 400/800/400 µmol CO_2 mol^{-1} air for 10/40/40 min under PPFD of 150 µmol m^{-2} s^{-1} (Medeiros et al., 2016). The half-times, expressed in min, for the stomatal kinetics curves were calculated as ln(2)/k. The rate constant, k, was fitted by non-linear fitting using the Microsoft Excel's Solver add-in as described previously (Martins et al., 2016).

Guard cell-enriched epidermal fragments and mesophyll cell protoplast isolation

The isolation of guard cell-enriched epidermal fragments was performed as described previously (Pandey et al., 2002). Briefly, fully expanded leaves from five rosettes per sample were blended for 1 min plus 1 min (twice for 30 s) using a warring blender (Phillips, RI 2044) with an internal filter to clarify the epidermal fragments of mesophyll and fibrous cells. Subsequently, epidermal fragments were collected on a nylon membrane (200 µm mesh) and washed to avoid apoplast contamination before being frozen in liquid nitrogen. This protocol resulted in a guard cell purity of approximately 98% (Antunes et al., 2012). For mesophyll cell protoplasts isolation, approximately 20 fully expanded leaves per replicate were harvested at the middle of the light period. The protoplasts were isolated using the TAPE-sandwich method as described by Wu et al. (2009).

qRT-PCR

qRT-PCR analysis was performed with total RNA isolated from mature leaves using the TRizol® reagent (Ambion, Life Technology) following the manufacturer's manual. For guard cell-enriched fragments and mesophyll cell protoplast the total RNA was isolated using the NucleoSpin® RNA Plant kit (MACHEREY-NAGEL GmbH & Co. KG). The integrity of the RNA was checked on 1% (w/v) agarose gels, and the concentration was measured using the system QIAxpert (QIAGEN). Digestion with DNase I (Amplication Grade DNase I, Invitrogen) was performed according to the manufacturer's instructions. Subsequently, total RNA was reverse transcribed into cDNA using Universal RiboClone® cDNA Synthesis System (Promega, Madison, WI, USA) according to the respective manufacturer's protocols. For analysis of gene expression, the Fast SYBR® Green PCR Master Mix

was used with the MicroAmp™ Optical 96-well Reaction Plate and MicroAmp™ Optical Adhesive Film (Applied Biosystems, Foster City, CA, USA). The relative expression levels were normalised using the constitutively expressed genes *F-BOX* and *TIP41-LIKE* (Czechowski et al., 2005), and calculated using the ΔCT method. The primers used for qRT-PCR were designed using the QuantPrime software (Messinger et al., 2006) or taken from those described by De Angeli et al. (2013). Detailed primers information is described in the Supplemental Table S1. The following genes were analysed: *ALUMINIUM ACTIVATED MALATE TRANSPORTER 6* and *9*, *ALMT6* and *ALMT9*; *QUICK ANION CHANNEL 1*, *QUAC1* (Medeiros et al., 2016); *ARABIDOPSIS THALIANA ATP-BINDING CASSETTE B14 AtABCB14* (Lee et al., 2008); *SLAC1*; H^+*-ATPASE 1* and *5*, *AHA1*, *AHA2*, and *AHA5* (Ueno et al., 2005); *POTASSIUM CHANNEL IN ARABIDOPSIS THALIANA 1*, *KAT1* (Nakamura et al., 1995) and *KAT2* (Pilot et al., 2001); K^+ *TRANSPORTER 1*, *AKT1* (Cao et al., 1995); the K^+ outflow channel *GATED OUTWARDLY-RECTIFYING* K^+ *CHANNEL,* GORK (Ache et al., 2000), and *TWO-PORE CHANNEL 1*, *TPC1* (Peiter et al., 2005).

Collection of apoplastic fluid and organic acids quantification

The leaf apoplastic fluid was collected as previously described with few modifications (Madsen et al., 2016). Briefly, six completely expanded leaves were cut with a razor blade and immediately submerged in deionized water to remove any surface contaminants at the middle of the light period. After, the leaves were submerged in the washing solution (deionized water). Then, applied vacuum to infiltrate the leaves (ca. -70 kPa) and released slowly (this procedure was repeated three times (1 min each) to give 100% of infiltration). After vacuum infiltration, leaf surfaces were completely and gently dried. Leaves were placed in a parafilm sheet, which was folded in such way that the leaves were stacked between layers of parafilm. Finally, this leaf-parafilm "sandwich" was mounted as described (Madsen et al., 2016) and after centrifugation in swinging buckets at 300 *g* for 10 min at 4 ºC the volume of apoplastic washing fluid was measured with a pipette. The apoplastic washing solutions were dried in lyophilizer. By using standards for citrate, malate, and fumarate we were able to quantify the absolute amount of these organic acids in the apoplastic fraction using an established GC-MS approach (Lisec et al., 2006),

Gas exchange and chlorophyll fluorescence measurements

Gas exchange parameters were determined simultaneously with chlorophyll *a* (Chl *a*) fluorescence measurements using the same gas exchange system described above. Instantaneous gas exchanges were measured after 1 h illumination during the light period under 150 µmol m^{-2} s^{-1} (light of growth) or 1000 µmol m^{-2} s^{-1} (light saturation) of photosynthetically active photon flux density (PPFD) at the leaf level. The reference CO_2 concentration was set at 400 µmol CO_2 mol^{-1} air. All measurements were performed using the 2 cm^2 leaf chamber at 25 °C, while the amount of blue light was set to 10% PPFD to optimize stomatal aperture.

All the Chl *a* fluorescence parameters were measured exactly as described in Medeiros et al. (2016). As the actual PSII photochemical efficiency (ϕ_{PSII}), estimated by chl *a* fluorescence parameters, represents the number of electrons transferred per photon absorbed in the PSII, the electron transport rate (J_{flu}) was calculated as $J_{flu} = \phi_{PSII} \cdot \alpha \cdot \beta \cdot PPFD$, where α is leaf absorptance and β reflects the partitioning of absorbed quanta between PSII and PSI, and the product $\alpha\beta$ was adopted as be in the literature to Arabidopsis 0.451 (Flexas et al., 2007).

Dark respiration (R_d) was measured using the same gas exchange system as described above after at least 1 h during the dark period and it was divided by two ($R_d/2$) to estimate the mitochondrial respiration rate in the light (R_L) (Niinemets et al., 2005, 2006; Niinemets et al., 2009).

Photosynthetic light-response curves *(A*/PPFD) were initiated at ambient CO_2 concentration (C_a) of 400 µmol mol^{-1} and PPFD of 1000 µmol m^{-2} s^{-1}. Then, the PPFD was increased to 1200 µmol m^{-2} s^{-1} and after decreased stepwise to 0 µmol m^{-2} s^{-1} (13 different PPFD steps). Simultaneously, Chl *a* fluorescence parameters were obtained (Yin et al., 2009). The responses of A_N to C_i (A_N /C_i curves) were performed at saturated light of 1000 µmol m^{-2} s^{-1} at 25°C under ambient O_2. Briefly, the measurements started at ambient CO_2 concentration (C_a) of 400 µmol mol^{-1} and when the steady state was reached, C_a was decreased stepwise to 50 µmol mol^{-1}. Upon completion of the measurements at low C_a, C_a was returned to 400 µmol mol^{-1} to restore the original A_N. Next, C_a was increased stepwise to 1600 µmol mol^{-1} in a total of 13 different C_a values (Long and Bernacchi, 2003).

689 **Estimation of mesophyll conductance (g_m), maximum rate of carboxylation**
690 **(V_{cmax}), maximum rate of carboxylation limited by electron transport (J_{max})**
691 **and photosynthetic limitations**
692
693 The concentration of CO_2 at the carboxylation sites (C_c) was calculated
694 following Harley et al. (1992) as :
695 $C_c = (\Gamma^* (J_{flu} + 8(A_N + R_L)))/(J_{flu} - 4(A_N + R_L))$
696 where the conservative value of Γ^* for Arabidopsis was taken from Mott et
697 al. (2008). Then, g_m was estimated as the slope of the A_N vs $C_i - C_c$ relationship as:
698 $g_m = A_N/(C_i - C_c)$
699 Thus, estimated g_m is an averaged value over the points used in the relationship (C_i
700 < 300 μmol mol^{-1}).
701 g_m was also estimated by a second method (Ethier and Livingston, 2004), which
702 fits A_N/C_i curves with a non-rectangular hyperbola version Farquhar–von Caemmerer–
703 Berry (FvCB) model, based on the hypothesis that g_m reduces the curvature of the
704 Rubisco-limited portion of an A_N/C_i curve.
705 From A_N/C_i and A_N/C_c curves, the maximum carboxylation velocity (V_{cmax}) and
706 the maximum capacity for electron transport rate (J_{max}) were calculated by fitting the
707 mechanistic model of CO_2 assimilation (Farquhar et al., 1980), using the C_i or C_c-based
708 temperature dependence of kinetic parameters of Rubisco (K_c and K_o) (Mott et al.,
709 2008). Then V_{cmax}, J_{max} and g_m were normalized to 25ºC using the temperature-response
710 equations from Sharkey et al. (2007).
711
712 **Determination of metabolite levels**
713 Whole rosettes were harvested in different times along of the light/dark cycle (0;
714 4; 8; 16; 24 h). Rosettes were flash frozen in liquid nitrogen and stored at -80 ºC until
715 further analyses. The levels of starch, sucrose, fructose, and glucose in the leaf
716 tissues were determined as described previously (Fernie et al., 2001). Malate and
717 fumarate were determined as detailed by Nunes-Nesi et al. (2007). The
718 photosynthetic pigments were determined as described (Porra et al., 1989). The
719 metabolite profiling was carried out in samples harvested at the middle of the day for
720 both leaves (Lisec et al., 2006) and guard cell-enriched epidermal fragments as
721 described previously (Daloso et al., 2015), with some modifications. Specifically, after
722 isolation the guard cell-enriched epidermal fragments were snap frozen in liquid

723 nitrogen and lyophilized for one week Approximately 30 mg of lyophilized guard
724 cell-enriched epidermal fragments were disrupted by shaking together with metal balls.
725 The extraction was performed using 1 mL of methanol and shaking (1000 rpm) at 70 ºC
726 for 15 min, 60 µL of Ribitol (0.2 mg mL^{-1}) was added as an internal standard. The
727 followed extraction and derivatization procedure was performed exactly as described
728 (Daloso et al., 2015). Peaks were manually annotated, and ion intensity was
729 determined by the aid of TagFinder software (Luedemann et al., 2012), using a
730 reference library from the Golm Metabolome Database (Kopka et al., 2005) and
731 following the recommended reporting format (Fernie et al., 2011).
732
733 **Non-aqueous fractionation (NAF)**
734 Five-week-old rosettes grown under short-day were harvested (pool of five
735 per replicate) in the middle of the light period, flash frozen, and ground to a fine
736 powder at -70 °C using a cryogenic grinding robot (Stitt et al., 2007), and stored at
737 -80 °C until further use. Approximately 4 g of powder were freeze-dried (-80 °C)
738 for one week. NAF was performed as described (Arrivault et al., 2014; Krueger et
739 al., 2014), and the gradient were divided into 8 fractions. After the last
740 centrifugation at 3,200 g (4 °C) for 10 min, the supernatant was discarded to
741 remove the solvent from the fractions. The pellet was resuspended in 7 mL of
742 heptane and divided into 6 aliquots of equal volumes. Finally, the suspension was
743 dried in a vacuum concentrator avoiding heating; aliquots were stored at -80 °C
744 until further use. Prior to analysis, the dried pellets were homogenized with the
745 appropriate extraction buffer by addition of one steel ball bearing and shaking at 25
746 Hz for 1 min in a ball mill (Retsch MM300, Retsch GmbH, Haan, Germany).
747 Enzyme and metabolite markers (adenosine diphosphate glucose pyrophosphorylase
748 and RubisCO activities for the chloroplast, phospho*enol*pyruvate carboxylase and
749 uridine diphosphate glucose pyrophosphorylase activities for the cytosol and acid
750 invertase activity and nitrate amounts for the vacuole) were determined as described
751 in Arrivault et al. (2014). Malate and fumarate were quantified via coupled
752 enzymatic assays (Cross et al., 2006). Citrate was quantified via enzymatic assay
753 adapted from (Tompkins and Toffaletti, 1982) in samples obtained with
754 chloroform/methanol/water extraction (Arrivault et al., 2009). Aliquots of extracts
755 (10 µl) or standards (10µl of 0, 125, 250, 500 µM, and 1 mM) were dispensed
756 directly into a microplate, followed by 100 µl 50 mM buffer (Tricine/KOH, pH 8)

containing 0.1 mM $ZnSO_4$, 0.5 mM NADH, 1.5 units malate dehydrogenase, 2.3 units lactate dehydrogenase. Absorbance was monitored at 340 nm until OD stabilized, 0.014 units citrate lyase added and absorbance monitored until stable. The other metabolites were measured using the GC-MS method also detailed above. Determination of subcellular distribution was performed using the BestFit software (Klie et al., 2011).

Enzyme activity measurements

The enzymatic extract was prepared as previously described (Gibon et al., 2004). Then, the maximum activities of PGK, PK, PFK, Aldolase, G6PH and Acid invertase were determined as described by Gibon et al. (2004); hexokinase, enolase, and TPI following Fernie et al. (2001); SuSy as in Zrenner et al. (1995); and transaldolase according to Debnam and Emes (1999).

TCA cycle flux on the basis of $^{14}CO_2$ evolution

Estimations of the TCA cycle flux on the basis of $^{14}CO_2$ evolution were performed following incubation of isolated leaf discs in 10 mM MES-KOH, pH 6.5, containing 0.3 mM Glc and supplied with 0.62 kBq mL^{-1} of [1-^{14}C]- and [3,4-^{14}C]-Glc under 150 µmol photons m^{-2} s^{-1}. The evolved $^{14}CO_2$ was trapped in KOH 10% (w/v) and quantified by liquid scintillation counter (Beckman LS 6500; Beckman Instruments, Fullerton, CA, USA). The results were interpreted following Rees and Beevers (1960).

Experimental design and statistical analysis

The data were obtained from the experiments using a completely randomized design using three genotypes, with the exception of the stomatal opening and closing kinetics, which were performed in randomized block design. All data are expressed as the mean ± standard error (SE). Data were tested for significant ($P < 0.05$) differences using Student's *t* tests. All the statistical analyses were performed using the algorithm embedded into Microsoft Excel® (Microsoft, Seattle).

Supplemental Data

Supplemental Fig. S1: Gene expression by semi quantitative RT-PCR.

Supplemental Fig. S2: Growth phenotype of WT and *tdt* plants.

Supplemental Fig. S3: Transcriptome data in leaves and guard cell manually dissected from Arabidopsis leaves.

Supplemental Fig. S4: Relative transcript levels of *tDT*.

Supplemental Fig. S5: Relative transcript levels of genes involved in organic and inorganic ion transport in guard cell.

Supplemental Fig. S6: Net photosynthesis (A_N) curves in response to substomatal (C_i) or chloroplastic (C_c) CO_2 concentrations in WT and *tdt* plants.

Supplemental Fig. S7: Total chlorophyll content ($a + b$) as well as the a/b ratio in WT and *tdt* plants.

Supplemental Fig. S8: Sugar content in WT and *tdt* plants.

Table S1: Primers utilized for the quantitative real time - PCR.

Table S2: Gas exchange and chlorophyll *a* fluorescence parameters in WT and *tdt* plants.

Table S3: Photosynthetic parameters from light-response curves in WT and *tdt* plants.

Table S4: Photosynthetic characterization of *tdt* mutant plants.

Table S5: Relative metabolite content for WT and *tdt* plants in leaves and guard cell-enriched epidermal fragments.

Table S6: Organic acids subcellular distribution.

Acknowledgements

The authors acknowledge Dr. Laíse Rosado, Ina Krahnert, and Manuela Guenther (all from the Max Planck Institute of Molecular Plant Physiology-MPIMP) for the helpful technical support. We are also grateful to Acácio Salvador for the excellent photographic work. Discussions with Prof. Mark Stitt and Dr. Saleh Alseekh (both from the MPIMP) regarding the NAF assays and GC-MS analysis, respectively, were highly valuable in the development of this work. We also thank Prof. Samuel V.C. Martins (Universidade Federal de Viçosa, Brazil) for useful discussions concerning gas exchange analyses.

Tables

Table I: Growth and morphology parameters in WT and *tdt* mutant plants. Data presented are mean ± SE (n = 6) obtained in two independent assays; values set in bold in *tdt* plants were determined by the Student's t test to be significantly different ($P < 0.05$) from WT.

Parameters*	WT	*tdt-1*	*tdt-2*
LA (cm^2)	53.8 ± 2.9	**44.1 ± 2.2**	**42.4 ± 2.3**
LDM (mg)	95.9 ± 4.2	**77.1 ± 5.7**	**72.2 ± 4.2**
RA (cm^2)	43.4 ± 1.5	**38.9 ± 1.3**	**34.9 ± 1.7**
RDM (mg)	122.2 ± 4.1	**93.6 ± 6.4**	**88.1 ± 5.5**
SLA ($m^2\ kg^{-1}$)	60.1 ± 1.3	57.9 ± 1.8	56.3 ± 0.9
SD (stomata mm^{-2})	270.9 ± 10.8	288.8 ± 3.4	273.8 ± 1.4
SI (%)	32.9 ± 1.3	31.4 ± 0.5	29.4 ± 0.9

*LA: total leaf area; LDM: leaves dry mass; RA: rosette area; RDM: Rosette dry mass; SLA: specific leaf area; SD: stomata density; SI: Stomatal Index.

Table II. Gas exchange and chlorophyll *a* fluorescence parameters in WT and *tdt* mutant plants measured under growth irradiance (150 µmol $m^{-2}\ s^{-1}$). Data presented are mean ± SE (n = 10) obtained in two independent assays (five plants in each assay).

Parameters*	WT	*tdt-1*	*tdt-2*
A_N (µmol $CO_2\ m^{-2}\ s^{-1}$)	5.4 ± 0.2	5.9 ± 0.1	5.6 ± 0.2
g_s (mol $H_2O\ m^{-2}\ s^{-1}$)	0.19 ± 0.01	0.18 ± 0.01	0.20 ± 0.01
E (mmol $H_2O\ m^{-2}\ s^{-1}$)	1.9 ± 0.2	1.7 ± 0.1	1.9 ± 0.2
F_v/F_m	0.78 ± 0.02	0.76 ± 0.01	0.75 ± 0.01

*A_N: Net photosynthesis; E: transpiration, g_s: stomatal conductance; F_v/F_m: PSII maximum photochemical efficiency

834 **Table III.** Enzyme activity analyses in WT and *tdt* plants. Activities were determined in
835 whole 5-weeks-old rosettes harvested at the middle of the light period. Values are
836 presented as means ± SE (n = 5); values in bold type in *tdt* plants were determined by
837 Student's t test to be significantly different ($P < 0.05$) from WT. FW, Fresh weight

Enzymes*	WT	*tdt-1*	*tdt-2*
Hexokinase[a]	13.3 ± 0.5	13.6 ± 0.7	14.7 ± 1.2
PGK[a]	10.5 ± 1.2	**14.5 ± 0.6**	**18.4 ± 0.5**
Pyruvate kinase[b]	105.6 ± 8.0	**162.2 ± 17.5**	**175.2 ± 9.6**
Phosphofructokinase[a]	1.6 ± 0.1	1.6 ± 0.1	1.8 ± 0.2
Enolase[a]	8.3 ± 0.5	7.6 ± 0.3	8.2 ± 0.2
TPI[a]	157.7 ± 8.1	144.0 ± 3.1	157.5 ± 4.4
Aldolase[b]	541.8 ± 39.1	676.4 ± 50.1	**837.2 ± 62.1**
Transaldolase[a]	2.0 ± 0.2	2.2 ± 0.1	1.6 ± 0.1
G6PDH[b]	221.9 ± 16.2	239.8 ± 10.2	269.7 ± 14.3
Sucrose synthase[b]	245.8 ± 16.8	234.0 ± 5.2	245.5 ± 19.0
Acid invertase[a]	46.0 ± 1.4	**32.2 ± 2.4**	**34.9 ± 1.5**

[a]Values expressed in μmol min^{-1} g^{-1} FW. [b]Values expressed in nmol min^{-1} g^{-1} FW
*Abbreviations: PGK: Phosphoglycerate kinase; TPI: Triose phosphate isomerase; G6PDH: Glucose-6- phosphate dehydrogenase.

838

839

Figure legends

Figure 1. Stomatal responses of *tdt* plant following different stimuli. Stomatal opening and closing kinetics in response to light and CO_2 concentrations. Stomatal conductance (g_s) was evaluated in *tdt-1* and *tdt-2* and WT in response to light **(A)**, dark **(B)** and CO_2 levels **(C)**. Data presented are mean ± SE (n = 10). **D**, Stomatal aperture after incubation with abscisic acid (ABA), malate, fumarate, and citrate. The 5th leaf totally expanded of 4-week-old plants were floated on stomatal opening buffer containing 10 mM KCl, 50 μM $CaCl_2$ and 5 mM MES-Tris (pH 6.15) for 2 h in the light (150 μmol m^{-2} s^{-1}) to pre-open stomata. After, ABA, malate, fumarate, and citrate or ethanol (solvent control) were added to the opening buffer. After more 2 h of incubation the stomatal aperture was then examined in the isolated epidermal fragments. Six leaves from different plants were evaluated and the apertures of at least 20 stomata per leaf were measured totalizing at least 120 stomata per genotype. Data are mean ± SE (n = 6) obtained in two independent experiments with comparable results. Asterisk indicates values that were determined by the Student's t test to be significantly different ($P < 0.05$) from WT.

Figure 2. Apoplastic concentrations of organic acids in *tdt* plants. The apoplastic concentrations of fumarate, malate, and malate were determined as described in Material and Methods section. Values are presented as means ± SE of six individual determinations per genotype. All measurements were performed in 5-week-old plants.

Figure 3. Starch and organic acid content in WT and *tdt* plants. **A** starch; **B** malate; and **C** fumarate content in whole rosettes harvested in different time points along of the light/dark cycle. Values are presented as mean ± SE (n = 6) and asterisk indicates the time where the values from mutant lines were determined by the Student's t test to be significantly different ($P < 0.05$) from WT.

Figure 4. Heat map representing the changes in relative metabolite content in leaves and guard cell-enriched epidermal fragments from WT and *tdt* plants. The full data sets from these metabolic profiling studies are additionally available in Supplemental Table S5. The colour code of the heat map is given at the log(2) following the scale above the diagram. Data are normalized with respect to the mean response calculated for WT (to allow statistical assessment, individual plants from this set were normalized in the same way). Values are presented as means ± SE (n = 5). Asterisks indicate that the values from mutant lines were determined by Student's t test to be significantly different ($P < 0.05$) from WT. In grey, the metabolites which were not detected or could not be annotated.

Figure 5. Respiration parameters in leaf disks from WT and *tdt* plants. $^{14}CO_2$ evolution from isolated leaf discs was determined under light conditions. The leaf discs were taken from 5-week-old plants and incubated in 10 mm MES–KOH solution, pH 6.5, 0.3 mM Glucose (Glc), 0.1 mM $CaSO_4$ supplemented with 0.62 kBq mL^{-1} of **(A)** [1-^{14}C]-Glc; or **(B)** [3,4-^{14}C]-Glc at an irradiance of 100 μmol m^{-2} s^{-1}. The $^{14}CO_2$ released was captured (at hourly intervals) in a KOH trap and the amount of radiolabel released was subsequently quantified by liquid scintillation counting. **C**, Ratio of carbon dioxide evolution from C3,4 to C1 positions of Glc in leaves of *tdt* plants. Values are presented as means ± SE (n = 3) **D**, Dark respiration measurements performed on 5-week-old plants. Values presented are mean ± SE (n = 10) obtained in two independent assays

887 (five plants in each assay). An asterisk indicates values that were determined by the
888 Student's *t* test to be significantly different ($P < 0.05$) from the WT plants.

889

890

Parsed Citations

Ache P, Becker D, Ivashikina N, Dietrich P, Roelfsema MRG, Hedrich R (2000) GORK, a delayed outward rectifier expressed in guard cells of Arabidopsis thaliana, is a K+-selective, K+-sensing ion channel. FEBS Letters 486: 93-98

Pubmed: Author and Title
CrossRef: Author and Title
Google Scholar: Author Only Title Only Author and Title

António C, Päpke C, Rocha M, Diab H, Limami AM, Obata T, Fernie AR, van Dongen JT (2016) Regulation of primary metabolism in response to low oxygen availability as revealed by carbon and nitrogen isotope redistribution. Plant Physiol 170: 43-56

Pubmed: Author and Title
CrossRef: Author and Title
Google Scholar: Author Only Title Only Author and Title

Antunes WC, Provart NJ, Williams TCR, Loureiro ME (2012) Changes in stomatal function and water use efficiency in potato plants with altered sucrolytic activity. Plant Cell Environ 35: 747-759

Pubmed: Author and Title
CrossRef: Author and Title
Google Scholar: Author Only Title Only Author and Title

Araújo WL, Nunes-Nesi A, Osorio S, Usadel B, Fuentes D, Nagy R, Balbo I, Lehmann M, Studart-Witkowski C, Tohge T, Martinoia E, Jordana X, DaMatta FM, Fernie AR (2011) Antisense inhibition of the iron-sulphur subunit of succinate dehydrogenase enhances photosynthesis and growth in tomato via an organic acid-mediated effect on stomatal aperture. Plant Cell 23: 600-627

Pubmed: Author and Title
CrossRef: Author and Title
Google Scholar: Author Only Title Only Author and Title

Arrivault S, Guenther M, Florian A, Encke B, Feil R, Vosloh D, Lunn JE, Sulpice R, Fernie AR, Stitt M, Schulze WX (2014) Dissecting the subcellular compartmentation of proteins and metabolites in Arabidopsis leaves using non-aqueous fractionation. Mol Cell Proteomics 13: 2246-2259

Pubmed: Author and Title
CrossRef: Author and Title
Google Scholar: Author Only Title Only Author and Title

Arrivault S, Guenther M, Ivakov A, Feil R, Vosloh D, Van Dongen JT, Sulpice R, Stitt M (2009) Use of reverse-phase liquid chromatography, linked to tandem mass spectrometry, to profile the Calvin cycle and other metabolic intermediates in Arabidopsis rosettes at different carbon dioxide concentrations. Plant J 59: 826-839

Pubmed: Author and Title
CrossRef: Author and Title
Google Scholar: Author Only Title Only Author and Title

Azoulay-Shemer T, Palomares A, Bagheri A, Israelsson-Nordstrom M, Engineer CB, Bargmann BOR, Stephan AB, Schroeder JI (2015) Guard cell photosynthesis is critical for stomatal turgor production, yet does not directly mediate CO2- and ABA-induced stomatal closing. Plant Journal 83: 567-581

Pubmed: Author and Title
CrossRef: Author and Title
Google Scholar: Author Only Title Only Author and Title

Bates GW, Rosenthal DM, Sun J, Chattopadhyay M, Peffer E, Yang J, Ort DR, Jones AM (2012) A comparative study of the Arabidopsis thaliana guard-cell transcriptome and its modulation by sucrose. PLoS One 7: e49641

Pubmed: Author and Title
CrossRef: Author and Title
Google Scholar: Author Only Title Only Author and Title

Berger D, Altmann T (2000) A subtilisin-like serine protease involved in the regulation of stomatal density and distribution in Arabidopsis thaliana. Genes Dev 14: 1119-1131

Pubmed: Author and Title
CrossRef: Author and Title
Google Scholar: Author Only Title Only Author and Title

Bolwell GP, Bindschedler LV, Blee KA, Butt VS, Davies DR, Gardner SL, Gerrish C, Minibayeva F (2002) The apoplastic oxidative burst in response to biotic stress in plants: a three-component system. J Exp Bot 53: 1367-1376

Pubmed: Author and Title
CrossRef: Author and Title
Google Scholar: Author Only Title Only Author and Title

Cao Y, Ward JM, Kelly WB, Ichida AM, Gaber RF, Anderson JA, Uozumi N, Schroeder JI, Crawford NM (1995) Multiple genes, tissue specificity, and expression-dependent modulation contribute to the functional diversity of potassium channels in Arabidopsis thaliana. Plant Physiol 109: 1093-1106

Pubmed: Author and Title
CrossRef: Author and Title
Google Scholar: Author Only Title Only Author and Title

Cross JM, von Korff M, Altmann T, Bartzetko L, Sulpice R, Gibon Y, Palacios N, Stitt M (2006) Variation of enzyme activities and

metabolite levels in 24 Arabidopsis accessions growing in carbon-limited conditions. Plant Physiol 142: 1574-1588
Pubmed: Author and Title
CrossRef: Author and Title
Google Scholar: Author Only Title Only Author and Title

Czechowski T, Stitt M, Altmann T, Udvardi MK, Scheible W-R (2005) Genome-wide identification and testing of superior reference genes for transcript normalization in Arabidopsis. Plant Physiol 139: 5-17
Pubmed: Author and Title
CrossRef: Author and Title
Google Scholar: Author Only Title Only Author and Title

Daloso DM, Antunes WC, Pinheiro DP, Waquim JP, Araújo WL, Loureiro ME, Fernie AR, Williams TCR (2015) Tobacco guard cells fix CO2 by both Rubisco and PEPcase while sucrose acts as a substrate during light-induced stomatal opening. Plant Cell Environ 38: 2353-2371
Pubmed: Author and Title
CrossRef: Author and Title
Google Scholar: Author Only Title Only Author and Title

De Angeli A, Zhang J, Meyer S, Martinoia E (2013) AtALMT9 is a malate-activated vacuolar chloride channel required for stomatal opening in Arabidopsis. Nat Commun 4: 1804
Pubmed: Author and Title
CrossRef: Author and Title
Google Scholar: Author Only Title Only Author and Title

Debnam PM, Emes MJ (1999) Subcellular distribution of enzymes of the oxidative pentose phosphate pathway in root and leaf tissues. J Exp Bot 50: 1653-1661
Pubmed: Author and Title
CrossRef: Author and Title
Google Scholar: Author Only Title Only Author and Title

Delhaize E, Gruber BD, Ryan PR (2007) The roles of organic anion permeases in aluminium resistance and mineral nutrition. FEBS Letters 581: 2255-2262
Pubmed: Author and Title
CrossRef: Author and Title
Google Scholar: Author Only Title Only Author and Title

Emmerlich V, Linka N, Reinhold T, Hurth MA, Traub M, Martinoia E, Neuhaus HE (2003) The plant homolog to the human sodium/dicarboxylic cotransporter is the vacuolar malate carrier. Proc Natl Acad Sci USA 100: 11122-11126
Pubmed: Author and Title
CrossRef: Author and Title
Google Scholar: Author Only Title Only Author and Title

Ethier GJ, Livingston NJ (2004) On the need to incorporate sensitivity to CO2 transfer conductance into the Farquhar-von Caemmerer-Berry leaf photosynthesis model. Plant Cell Environ 27: 137-153
Pubmed: Author and Title
CrossRef: Author and Title
Google Scholar: Author Only Title Only Author and Title

Fahnenstich H, Saigo M, Niessen M, Zanor MI, Andreo CS, Fernie AR, Drincovich MF, Flügge U-I, Maurino VG (2007) Alteration of organic acid metabolism in Arabidopsis overexpressing the maize C4 NADP-Malic Enzyme causes accelerated senescence during extended darkness. Plant Physiol 145: 640-652
Pubmed: Author and Title
CrossRef: Author and Title
Google Scholar: Author Only Title Only Author and Title

Farquhar GD, von Caemmerer S, Berry JA (1980) A biochemical model of photosynthetic CO2 assimilation in leaves of C3 species. Planta 149: 78-90
Pubmed: Author and Title
CrossRef: Author and Title
Google Scholar: Author Only Title Only Author and Title

Fernie AR, Aharoni A, Willmitzer L, Stitt M, Tohge T, Kopka J, Carroll AJ, Saito K, Fraser PD, DeLuca V (2011) Recommendations for reporting metabolite data. The Plant Cell 23: 2477-2482
Pubmed: Author and Title
CrossRef: Author and Title
Google Scholar: Author Only Title Only Author and Title

Fernie AR, Carrari F, Sweetlove LJ (2004) Respiratory metabolism: glycolysis, the TCA cycle and mitochondrial electron transport. Curr Opin Plant Biol 7: 254-261
Pubmed: Author and Title
CrossRef: Author and Title
Google Scholar: Author Only Title Only Author and Title

Fernie AR, Roscher A, Ratcliffe RG, Kruger NJ (2001) Fructose 2,6-bisphosphate activates pyrophosphate: fructose-6-phosphate 1-phosphotransferase and increases triose phosphate to hexose phosphate cycling in heterotrophic cells. Planta 212: 250-263

Pubmed: Author and Title
CrossRef: Author and Title
Google Scholar: Author Only Title Only Author and Title

Figueroa CM, Feil R, Ishihara H, Watanabe M, Kölling K, Krause U, Höhne M, Encke B, Plaxton WC, Zeeman SC, Li Z, Schulze WX, Hoefgen R, Stitt M, Lunn JE (2016) Trehalose 6-phosphate coordinates organic and amino acid metabolism with carbon availability. Plant J 85: 410-423
Pubmed: Author and Title
CrossRef: Author and Title
Google Scholar: Author Only Title Only Author and Title

Finkemeier I, König A-C, Heard W, Nunes-Nesi A, Pham PA, Leister D, Fernie AR, Sweetlove LJ (2013) Transcriptomic analysis of the role of carboxylic acids in metabolite signaling in Arabidopsis leaves. Plant Physiol 162: 239-253
Pubmed: Author and Title
CrossRef: Author and Title
Google Scholar: Author Only Title Only Author and Title

Flexas J, Ortuno MF, Ribas-Carbo M, Diaz-Espejo A, Florez-Sarasa ID, Medrano H (2007) Mesophyll conductance to CO2 in Arabidopsis thaliana. New Phytol 175: 501-511
Pubmed: Author and Title
CrossRef: Author and Title
Google Scholar: Author Only Title Only Author and Title

Gerhardt R, Stitt M, Heldt HW (1987) Subcellular metabolite levels in spinach leaves: regulation of sucrose synthesis during diurnal alterations in photosynthetic partitioning. Plant Physiol 83: 399-407
Pubmed: Author and Title
CrossRef: Author and Title
Google Scholar: Author Only Title Only Author and Title

Gibon Y, Blaesing OE, Hannemann J, Carillo P, Hohne M, Hendriks JH, Palacios N, Cross J, Selbig J, Stitt M (2004) A Robot-based platform to measure multiple enzyme activities in Arabidopsis using a set of cycling assays: comparison of changes of enzyme activities and transcript levels during diurnal cycles and in prolonged darkness. Plant Cell 16: 3304-3325
Pubmed: Author and Title
CrossRef: Author and Title
Google Scholar: Author Only Title Only Author and Title

Gibon Y, Pyl E-T, Sulpice R, Lunn JE, Höhne M, Günther M, Stitt M (2009) Adjustment of growth, starch turnover, protein content and central metabolism to a decrease of the carbon supply when Arabidopsis is grown in very short photoperiods. Plant Cell Environ 32: 859-874
Pubmed: Author and Title
CrossRef: Author and Title
Google Scholar: Author Only Title Only Author and Title

Harley PC, Loreto F, Di Marco G, Sharkey TD (1992) Theoretical considerations when estimating the mesophyll conductance to CO2 flux by analysis of the response of photosynthesis to CO2. Plant Physiol 98: 1429-1436
Pubmed: Author and Title
CrossRef: Author and Title
Google Scholar: Author Only Title Only Author and Title

Hedrich R, Marten I (1993) Malate-induced feedback regulation of plasma membrane anion channels could provide a CO2 sensor to guard-cells. EMBO J 12: 897-901
Pubmed: Author and Title
CrossRef: Author and Title
Google Scholar: Author Only Title Only Author and Title

Hedrich R, Marten I, Lohse G, Dietrich P, Winter H, Lohaus G, Heldt HW (1994) Malate-sensitive anion channels enable guard cells to sense changes in the ambient CO2 concentration. Plant J 6: 741-748
Pubmed: Author and Title
CrossRef: Author and Title
Google Scholar: Author Only Title Only Author and Title

Hunt R, Causton DR, Shipley B, Askew AP (2002) A modern tool for classical plant growth analysis. Ann Bot 90: 485-488
Pubmed: Author and Title
CrossRef: Author and Title
Google Scholar: Author Only Title Only Author and Title

Hurth MA, Suh SJ, Kretzschmar T, Geis T, Bregante M, Gambale F, Martinoia E, Neuhaus HE (2005) Impaired pH homeostasis in Arabidopsis lacking the vacuolar dicarboxylate transporter and analysis of carboxylic acid transport across the tonoplast. Plant Physiol 137: 901-910
Pubmed: Author and Title
CrossRef: Author and Title
Google Scholar: Author Only Title Only Author and Title

Kim T-H, Böhmer M, Hu H, Nishimura N, Schroeder JI (2010) Guard cell signal transduction network: advances in understanding abscisic acid, CO2, and Ca2+ signaling. Annu Rev Plant Biol 61: 561-591

Pubmed: Author and Title
CrossRef: Author and Title
Google Scholar: Author Only Title Only Author and Title

Klie S, Krueger S, Krall L, Giavalisco P, Flügge U-I, Willmitzer L, Steinhauser D (2011) Analysis of the compartmentalized metabolome - A validation of the non-aqueous fractionation technique. Front Plant Sci 2: 55

Pubmed: Author and Title
CrossRef: Author and Title
Google Scholar: Author Only Title Only Author and Title

Kopka J, Schauer N, Krueger S, Birkemeyer C, Usadel B, Bergmüller E, Dörmann P, Weckwerth W, Gibon Y, Stitt M, Willmitzer L, Fernie AR, Steinhauser D (2005) GMD@CSB.DB: the Golm Metabolome Database. Bioinformatics 21: 1635-1638

Pubmed: Author and Title
CrossRef: Author and Title
Google Scholar: Author Only Title Only Author and Title

Kovermann P, Meyer S, Hörtensteiner S, Picco C, Scholz-Starke J, Ravera S, Lee Y, Martinoia E (2007) The Arabidopsis vacuolar malate channel is a member of the ALMT family. Plant J 52: 1169-1180

Pubmed: Author and Title
CrossRef: Author and Title
Google Scholar: Author Only Title Only Author and Title

Krueger S, Steinhauser D, Lisec J, Giavalisco P (2014) Analysis of subcellular metabolite distributions within Arabidopsis thaliana leaf tissue: A primer for subcellular metabolomics. Methods Mol. Biol. 1062: 575-596

Pubmed: Author and Title
CrossRef: Author and Title
Google Scholar: Author Only Title Only Author and Title

Lauxmann MA, Annunziata MG, Brunoud G, Wahl V, Koczut A, Burgos A, Olas JJ, Maximova E, Abel C, Schlereth A, Soja AM, Bläsing OE, Lunn JE, Vernoux T, Stitt M (2016) Reproductive failure in Arabidopsis thaliana under transient carbohydrate limitation: flowers and very young siliques are jettisoned and the meristem is maintained to allow successful resumption of reproductive growth. Plant Cell Environ 39: 745-767

Pubmed: Author and Title
CrossRef: Author and Title
Google Scholar: Author Only Title Only Author and Title

Lee M, Choi Y, Burla B, Kim YY, Jeon B, Maeshima M, Yoo JY, Martinoia E, Lee Y (2008) The ABC transporter AtABCB14 is a malate importer and modulates stomatal response to CO2. Nat Cell Biol 10: 1217-1223

Pubmed: Author and Title
CrossRef: Author and Title
Google Scholar: Author Only Title Only Author and Title

Lisec J, Schauer N, Kopka J, Willmitzer L, Fernie AR (2006) Gas chromatography mass spectrometry-based metabolite profiling in plants. Nature Protocols 1: 387-396

Pubmed: Author and Title
CrossRef: Author and Title
Google Scholar: Author Only Title Only Author and Title

Lohaus G, Pennewiss K, Sattelmacher B, Hussmann M, Hermann Muehling K (2001) Is the infiltration-centrifugation technique appropriate for the isolation of apoplastic fluid? A critical evaluation with different plant species. Physiol Plant 111: 457-465

Pubmed: Author and Title
CrossRef: Author and Title
Google Scholar: Author Only Title Only Author and Title

Long SP, Bernacchi CJ (2003) Gas exchange measurements, what can they tell us about the underlying limitations to photosynthesis? Procedures and sources of error. J Exp Bot 54: 2393-2401

Pubmed: Author and Title
CrossRef: Author and Title
Google Scholar: Author Only Title Only Author and Title

Luedemann A, von Malotky L, Erban A, Kopka J (2012) TagFinder: Preprocessing Software for the Fingerprinting and the Profiling of Gas Chromatography-Mass Spectrometry Based Metabolome Analyses. In NW Hardy, RD Hall, eds, Plant Metabolomics: Methods and Protocols. Humana Press, Totowa, NJ, pp 255-286

Pubmed: Author and Title
CrossRef: Author and Title
Google Scholar: Author Only Title Only Author and Title

Madsen SR, Nour-Eldin HH, Halkier BA (2016) Collection of apoplastic fluids from Arabidopsis thaliana Leaves. In GA Fett-Neto, ed, Biotechnology of plant secondary metabolism: Methods and Protocols. Springer New York, New York, NY, pp 35-42

Pubmed: Author and Title
CrossRef: Author and Title
Google Scholar: Author Only Title Only Author and Title

Maier A, Zell MB, Maurino VG (2011) Malate decarboxylases: evolution and roles of NAD(P)-ME isoforms in species performing C4 and C3 photosynthesis. J Exp Bot 62: 3061-3069

Pubmed: Author and Title
CrossRef: Author and Title
Google Scholar: Author Only Title Only Author and Title

Martinoia E, Rentsch D (1994) Malate compartmentation - responses to a complex metabolism. Annu Rev Plant Physiol Plant Mol Biol 45: 447-467

Pubmed: Author and Title
CrossRef: Author and Title
Google Scholar: Author Only Title Only Author and Title

Martins SCV, Galmés J, Molins A, DaMatta FM (2013) Improving the estimation of mesophyll conductance to CO2: on the role of electron transport rate correction and respiration. J Exp Bot 64: 1-14

Pubmed: Author and Title
CrossRef: Author and Title
Google Scholar: Author Only Title Only Author and Title

Martins SCV, McAdam SA, Deans RM, DaMatta FM, Brodribb TJ (2016) Stomatal dynamics are limited by leaf hydraulics in ferns and conifers: results from simultaneous measurements of liquid and vapour fluxes in leaves. Plant Cell Environ 39: 694-705

Pubmed: Author and Title
CrossRef: Author and Title
Google Scholar: Author Only Title Only Author and Title

Medeiros DB, Martins SCV, Cavalcanti JHF, Daloso DM, Martinoia E, Nunes-Nesi A, DaMatta FM, Fernie AR, Araújo WL (2016) Enhanced photosynthesis and growth in atquac1 knockout mutants are due to altered organic acid accumulation and an increase in both stomatal and mesophyll conductance. Plant Physiol 170: 86-101

Pubmed: Author and Title
CrossRef: Author and Title
Google Scholar: Author Only Title Only Author and Title

Messinger SM, Buckley TN, Mott KA (2006) Evidence for involvement of photosynthetic processes in the stomatal response to CO2. Plant Physiol 140: 771-778

Pubmed: Author and Title
CrossRef: Author and Title
Google Scholar: Author Only Title Only Author and Title

Meyer S, Scholz-Starke J, De Angeli A, Kovermann P, Burla B, Gambale F, Martinoia E (2011) Malate transport by the vacuolar AtALMT6 channel in guard cells is subject to multiple regulation. Plant J 67: 247-257

Pubmed: Author and Title
CrossRef: Author and Title
Google Scholar: Author Only Title Only Author and Title

Mott KA, Sibbernsen ED, Shope JC (2008) The role of the mesophyll in stomatal responses to light and CO2. Plant Cell Environ 31: 1299-1306

Pubmed: Author and Title
CrossRef: Author and Title
Google Scholar: Author Only Title Only Author and Title

Nakamura RL, McKendree Jr WL, Hirsch RE, Sedbrook JC, Gaber RF, Sussman MR (1995) Expression of an Arabidopsis potassium channel gene in guard cells. Plant Physiol 109: 371-374

Pubmed: Author and Title
CrossRef: Author and Title
Google Scholar: Author Only Title Only Author and Title

Negi J, Matsuda O, Nagasawa T, Oba Y, Takahashi H, Kawai-Yamada M, Uchimiya H, Hashimoto M, Iba K (2008) CO2 regulator SLAC1 and its homologues are essential for anion homeostasis in plant cells. Nature 452: 483-486

Pubmed: Author and Title
CrossRef: Author and Title
Google Scholar: Author Only Title Only Author and Title

Niinemets Ü, Cescatti A, Rodeghiero M, Tosens T (2005) Leaf internal diffusion conductance limits photosynthesis more strongly in older leaves of Mediterranean evergreen broad-leaved species. Plant Cell Environ 28: 1552-1566

Pubmed: Author and Title
CrossRef: Author and Title
Google Scholar: Author Only Title Only Author and Title

Niinemets Ü, Cescatti A, Rodeghiero M, Tosens T (2006) Complex adjustments of photosynthetic potentials and internal diffusion conductance to current and previous light availabilities and leaf age in Mediterranean evergreen species Quercus ilex. Plant Cell Environ 29: 1159-1178

Pubmed: Author and Title
CrossRef: Author and Title
Google Scholar: Author Only Title Only Author and Title

Niinemets Ü, Díaz-Espejo A, Flexas J, Galmés J, Warren CR (2009) Role of mesophyll diffusion conductance in constraining potential photosynthetic productivity in the field. Journal of Experimental Botany 60: 2249-2270

Pubmed: Author and Title

CrossRef: Author and Title
Google Scholar: Author Only Title Only Author and Title

Nunes-Nesi A, Araújo WL, Fernie AR (2011) Targeting mitochondrial metabolism and machinery as a means to enhance photosynthesis. Plant Physiol 155: 101-107
Pubmed: Author and Title
CrossRef: Author and Title
Google Scholar: Author Only Title Only Author and Title

Nunes-Nesi A, Carrari F, Gibon Y, Sulpice R, Lytovchenko A, Fisahn J, Graham J, Ratcliffe RG, Sweetlove LJ, Fernie AR (2007) Deficiency of mitochondrial fumarase activity in tomato plants impairs photosynthesis via an effect on stomatal function. Plant J 50: 1093-1106
Pubmed: Author and Title
CrossRef: Author and Title
Google Scholar: Author Only Title Only Author and Title

Pandey S, Wang X-Q, Coursol SA, Assmann SM (2002) Preparation and applications of Arabidopsis thaliana guard cell protoplasts. New Phytol 153: 517-526
Pubmed: Author and Title
CrossRef: Author and Title
Google Scholar: Author Only Title Only Author and Title

Peiter E, Maathuis FJM, Mills LN, Knight H, Pelloux J, Hetherington AM, Sanders D (2005) The vacuolar Ca2+-activated channel TPC1 regulates germination and stomatal movement. Nature 434: 404-408
Pubmed: Author and Title
CrossRef: Author and Title
Google Scholar: Author Only Title Only Author and Title

Pilot G, Lacombe Bt, Gaymard F, Chérel I, Boucherez J, Thibaud J-B, Sentenac H (2001) Guard cell inward K+ channel activity in Arabidopsis involves expression of the twin channel subunits KAT1 and KAT2. J Biol Chem 276: 3215-3221
Pubmed: Author and Title
CrossRef: Author and Title
Google Scholar: Author Only Title Only Author and Title

Porra RJ, Thompson WA, Kriedemann PE (1989) Determination of accurate extinction coefficients and simultaneous equations for assaying chlorophylls a and b extracted with four different solvents: verification of the concentration of chlorophyll standards by atomic absorption spectroscopy. BBA - Bioenergetics 975: 384-394
Pubmed: Author and Title
CrossRef: Author and Title
Google Scholar: Author Only Title Only Author and Title

Raschke K (2003) Alternation of the slow with the quick anion conductance in whole guard cells effected by external malate. Planta 217: 651-657
Pubmed: Author and Title
CrossRef: Author and Title
Google Scholar: Author Only Title Only Author and Title

Rees TA, Beevers H (1960) Pathways of glucose dissimilation in carrot slices. Plant Physiol 35: 830-838
Pubmed: Author and Title
CrossRef: Author and Title
Google Scholar: Author Only Title Only Author and Title

Santelia D, Lawson T (2016) Rethinking guard cell metabolism. Plant Physiol 172: 1371-1392
Pubmed: Author and Title
CrossRef: Author and Title
Google Scholar: Author Only Title Only Author and Title

Schindelin J, Rueden CT, Hiner MC, Eliceiri KW (2015) The ImageJ ecosystem: An open platform for biomedical image analysis. Molecular Reproduction and Development 82: 518-529
Pubmed: Author and Title
CrossRef: Author and Title
Google Scholar: Author Only Title Only Author and Title

Sharkey TD, Bernacchi CJ, Farquhar GD, Singsaas EL (2007) Fitting photosynthetic carbon dioxide response curves for C3 leaves. Plant Cell Environ 30: 1035-1040
Pubmed: Author and Title
CrossRef: Author and Title
Google Scholar: Author Only Title Only Author and Title

Stitt M, Sulpice R, Gibon Y, Whitwell A, Skilbeck R, Parker S, Ellison R (2007) Cryogenic grinder system. Germany patent number 08146.0025U1. In,
Pubmed: Author and Title
CrossRef: Author and Title
Google Scholar: Author Only Title Only Author and Title

Sulpice R, Flis A, Ivakov AA, Apelt F, Krohn N, Encke B, Abel C, Feil R, Lunn JE, Stitt M (2014) Arabidopsis coordinates the diurnal

regulation of carbon allocation and growth across a wide range of photoperiods. Molecular Plant 7: 137-155
Pubmed: Author and Title
CrossRef: Author and Title
Google Scholar: Author Only Title Only Author and Title

Sweetlove LJ, Beard KFM, Nunes-Nesi A, Fernie AR, Ratcliffe RG (2010) Not just a circle: flux modes in the plant TCA cycle. Trends Plant Sci 15: 462-470
Pubmed: Author and Title
CrossRef: Author and Title
Google Scholar: Author Only Title Only Author and Title

Tompkins D, Toffaletti J (1982) Enzymic determination of citrate in serum and urine, with use of the Worthington "ultrafree" device. Clin Chem 28: 192-195
Pubmed: Author and Title
CrossRef: Author and Title
Google Scholar: Author Only Title Only Author and Title

Tronconi MA, Fahnenstich H, Gerrard Weehler MC, Andreo CS, Flügge U-I, Drincovich MF, Maurino VG (2008) Arabidopsis NAD-Malic enzyme functions as a homodimer and heterodimer and has a major impact on nocturnal metabolism. Plant Physiol 146: 1540-1552
Pubmed: Author and Title
CrossRef: Author and Title
Google Scholar: Author Only Title Only Author and Title

Ueno K, Kinoshita T, Inoue S-i, Emi T, Shimazaki K-i (2005) Biochemical characterization of plasma membrane H+-ATPase ativation in guard cell protoplasts of Arabidopsis thaliana in response to blue light. Plant Cell Physiol 46: 955-963
Pubmed: Author and Title
CrossRef: Author and Title
Google Scholar: Author Only Title Only Author and Title

Von Groll U, Berger D, Altmann T (2002) The subtilisin-like serine protease SDD1 mediates cell-to-cell signaling during Arabidopsis stomatal development. The Plant Cell 14: 1527-1539
Pubmed: Author and Title
CrossRef: Author and Title
Google Scholar: Author Only Title Only Author and Title

Weisskopf L, Abou-Mansour E, Fromin N, Tomasi N, Santelia D, Edelkott I, Neumann G, Aragno M, Tabacchi R, Martinoia E (2006) White lupin has developed a complex strategy to limit microbial degradation of secreted citrate required for phosphate acquisition. Plant Cell Environ 29: 919-927
Pubmed: Author and Title
CrossRef: Author and Title
Google Scholar: Author Only Title Only Author and Title

Winter H, Robinson DG, Heldt HW (1993) Subcellular volumes and metabolite concentrations in barley leaves. Planta 191: 180-190
Pubmed: Author and Title
CrossRef: Author and Title
Google Scholar: Author Only Title Only Author and Title

Winter H, Robinson DG, Heldt HW (1994) Subcellular volumes and metabolite concentrations in spinach leaves. Planta 193: 530-535
Pubmed: Author and Title
CrossRef: Author and Title
Google Scholar: Author Only Title Only Author and Title

Wu F-H, Shen S-C, Lee L-Y, Lee S-H, Chan M-T, Lin C-S (2009) Tape-Arabidopsis Sandwich - a simpler Arabidopsis protoplast isolation method. Plant Methods 5: 16
Pubmed: Author and Title
CrossRef: Author and Title
Google Scholar: Author Only Title Only Author and Title

Yin X, Struik PC, Romero P, Harbinson J, Evers JB, Van Der Putten PEL, Vos JAN (2009) Using combined measurements of gas exchange and chlorophyll fluorescence to estimate parameters of a biochemical C3 photosynthesis model: a critical appraisal and a new integrated approach applied to leaves in a wheat (Triticum aestivum) canopy. Plant Cell Environ 32: 448-464
Pubmed: Author and Title
CrossRef: Author and Title
Google Scholar: Author Only Title Only Author and Title

Zell MB, Fahnenstich H, Maier A, Saigo M, Voznesenskaya EV, Edwards GE, Andreo C, Schleifenbaum F, Zell C, Drincovich MF, Maurino VG (2010) Analysis of Arabidopsis with highly reduced levels of malate and fumarate sheds light on the role of these organic acids as storage carbon molecules. Plant Physiol 152: 1251-1262
Pubmed: Author and Title
CrossRef: Author and Title
Google Scholar: Author Only Title Only Author and Title

Zrenner R, Salanoubat M, Willmitzer L, Sonnewald U (1995) Evidence of the crucial role of sucrose synthase for sink strength using transgenic potato plants (Solanum tuberosum L.). Plant J 7: 97-107
Pubmed: Author and Title